Contents lists available at ScienceDirect

Polymer Degradation and Stability

A multi-technique and multi-scale analysis of the thermal degradation of PEEK in laser heating

Dimitrios Gaitanelis [a,b,*], Angeliki Chanteli [c], Chris Worrall [d], Paul M. Weaver [c], Mihalis Kazilas [e]

[a] Advanced Manufacturing Research Centre with Boeing, University of Sheffield, Catcliff, Rotherham S60 5TZ, United Kingdom
[b] NSIRC, TWI Ltd, Granta Park, Great Abington, Cambridge, CB21 6AL, United Kingdom
[c] Bernal Institute, School of Engineering, University of Limerick, Ireland
[d] Advanced Composites and Adhesives Section (ACA), TWI Ltd, Cambridge, CB21 6AL, United Kingdom
[e] Brunel Composites Centre (BCC), Brunel University London, London, Uxbridge UB8 3PH, United Kingdom

ARTICLE INFO

ABSTRACT

The present work studies the thermal degradation of laser-heated poly-ether-ether-ketone (PEEK) as the heating duration increases. Its damage morphology, chemical composition, crystallinity content, and mechanical properties are examined with optical microscopy, attenuated total reflection-Fourier transform infrared spectroscopy, differential scanning calorimetry, Raman spectroscopy, and continuous stiffness measurement nanoindentation. The applicability of those methods in detecting the thermal degradation of laser-heated PEEK and assessing the induced thermal damage is highlighted. Results show that short-time laser heating acts as an annealing process that improves the crystallinity and hardness on the affected surface of PEEK by up to 5.1% and 10.8% respectively. With a further increase in the heating duration, surface carbonisation occurs and a char layer is formed. Surface carbonisation is associated with the thermal limits of PEEK in laser heating decreasing by up to 50% its hardness and by 45% its indentation modulus. Finally, the char layer is found to act as a shielding mechanism that protects the bulk PEEK from the applied thermal load, resulting in mostly superficial thermally induced damage.

1. Introduction

The growing implementation of high-power lasers in composites manufacturing has increased the interest of industry and academia in the laser heating of poly-ether-ether-ketone (PEEK) and of carbon fibre (CF) reinforced PEEK [1–5]. Applications of CF/PEEK where continuous wave (CW) lasers are used, such as laser-assisted tape placement (LATP), are increasingly studied to enhance its use in the aerospace industry [1–3,6–11]. Furthermore, in medical applications laser surface texturing is commonly applied, to improve the adhesive bonding properties and/or tailor the wettability of pure PEEK [12]. Usually, pulsed laser heating of up to a few ns is employed in these applications to modify the surface of PEEK [13–20].

Despite the growing use of laser heating in PEEK and CF/PEEK, there is currently a lack of studies examining their thermal degradation mechanisms in these conditions. Most works have focused on the degradation of PEEK after thermal ageing [21,22] or long-time heating [23–25]. Recently, research groups have examined its response in rapid

high-temperature processing [26] and in processing cycles that are shorter than 5 min [27]. A few studies have been reported that examined the thermal degradation of laser-heated PEEK [28], and there is little work that has highlighted suitable techniques for detecting and assessing the induced thermal damage in these conditions [29]. However, short-time laser heating of a few ms could benefit the laser applications of PEEK especially when it is accompanied by high power densities. Studies have shown that an increased laser irradiance for a shorter amount of time results in a lower mass loss than in applications where laser processing of lower heating rates is involved [30,31]. These processing conditions could increase the temperatures reached by the material without inducing significant thermal damage on its surface and could thus further expand the process window of PEEK in laser processing. Therefore, it is important to investigate the thermal limits of PEEK in short-time laser heating of a few ms with increased power densities.

One of the main challenges in these conditions is to measure experimentally the resulting temperatures [26,32]. Additionally, even if

---

* Corresponding author.
  E-mail address: d.gaitanelis@sheffield.ac.uk (D. Gaitanelis).

the exact temperatures are captured they cannot necessarily answer whether thermal damage is induced in the material. Considering the extreme heating rates that are applied, the smaller amount of time that the polymer would remain at elevated temperatures might not be sufficient to trigger the thermal degradation mechanisms of laser-heated PEEK. To be able to answer that, it is important to employ suitable degradation detection techniques that could assess the thermal damage that occurs in laser-heated PEEK.

To do so, a multi-technique and multi-scale analysis takes place to examine the response of PEEK in laser heating. PEEK samples are laser heated with a Gaussian beam of a 5 mm spot diameter, a power of 600 W, and a heating duration that varies between 1 ms and 14 ms. Several experimental methods are applied to examine the damage morphology, chemical composition, crystallinity content, and mechanical properties of laser-heated PEEK. Optical microscopy (OM) investigates the thermal damage formation pattern as the applied heating duration increases. Attenuated total reflection - Fourier transform infrared spectroscopy (ATR-FTIR) identifies the spectral changes that occur on laser-heated PEEK, and the 1305/1280 cm^{-1} IR bands intensity ratio is examined to assess its crystallinity content [33]. Raman spectroscopy and differential scanning calorimetry (DSC) also assess the crystallinity of PEEK at the micro- and bulk material level respectively, and continuous stiffness measurement (CSM) nanoindentation investigates the laser heating effect on its mechanical properties. Through this process, the degradation mechanisms that occur in laser-heated PEEK are thoroughly examined, and a methodology is introduced that can detect whether the applied laser heating induces thermal damage on the surface of PEEK or it improves its superficial properties. This study's examined material and applied methods are described in Section 2. In Section 3, the results of each investigation are presented and discussed, and the main conclusions are gathered in Section 4.

2. Materials and methods

2.1. Examined material and laser experiment

The examined PEEK samples have a thickness of 0.5 mm and their density is equal to 1.3 g/cm^3. They are supplied by Engineering & Design Plastics Ltd., Cambridge, UK and have a glass transition temperature (T_g) of 147 °C $\pm$ 0.1 °C and a melting point (T_m) equal to 338.7 °C $\pm$ 0.07 °C. The laser heating experiment takes place with an IPG YLS-5000 CW fiber laser with a maximum power of 5000 W and a wavelength of 1070 nm. A focal length of 160 mm is used and the defocus distance is equal to +42 mm, so the nominal spot diameter would equal 5 mm. The defocused beam is similar to a Gaussian distribution and can be best approximated by a frustum shape [34], and in this work, the PEEK samples are heated with a laser power equal to 600 W for a heating duration that varies between 1 ms and 14 ms. Recent investigations have identified that PEEK does not strongly absorb the laser heat flux at 1070 nm [35]. Nevertheless, this study aims to understand the thermal degradation of PEEK at extreme heating rates and short exposure times, and introduce an experimental methodology that can be relevant for a range of applications where these processing conditions are used (e.g. induction heating [36]). Therefore, an investigation into the optimisation of the laser beam and the amount of energy absorbed by the polymer was not part of the study.

2.2. Methods

2.2.1. Optical microscopy

To examine the effect of the applied laser heating on the surface and through the thickness of PEEK, the laser-heated PEEK samples are examined with OM. An Olympus Optical Microscope is used, equipped with a set of available magnification lenses of 2.5×, 5×, 10×, 20×, and 50×. Through this process, the thermally affected area of each sample is identified and the critical regions where the nanoindentation and

Raman spectroscopy measurements take place are detected.

2.2.2. ATR-FTIR

To identify the spectral changes that occur in laser-heated PEEK, a Nicolet iS50 FTIR spectrometer provided by Thermo Fischer Scientific Inc. is used, equipped with a built-in diamond ATR. A resolution of 4 cm^{-1} is applied and the accumulated spectra are collected from 4000 to 600 cm^{-1} with 128 scans. Each sample is examined five times, and the spectra are baseline-corrected and normalised to the phenyl ring stretching peak at 1593 cm^{-1}, which was the strongest at the examined heating conditions. Through this process, the main degradation mechanisms are identified as the heating duration increases.

In addition, the intensity ratio of the 1305/1280 cm^{-1} IR bands is examined. Chalmers et al. were the first research group that correlated the 1305/1280 cm^{-1} intensity ratio of PEEK with its degree of crystallinity (DOC) [33,37,38]. Since then, a number of studies have used this method to examine the DOC of PEEK after an applied thermal treatment [12,39,40]. Regis et al. examined the crystallinity of PEEK after an annealing treatment with both the 1305/1280 cm^{-1} intensity ratio and DSC and they also identified a good agreement between the two methods [39]. Recently, it has been used for assessing the DOC of PEEK after femtosecond laser processing [40] and after laser treatment that aimed to improve its tribological performance under seawater lubrication [12]. Likewise, to identify the crystallinity of laser-heated PEEK as the heating duration increases, the 1305/1280 cm^{-1} intensity ratio is examined according to the ASTM F2778-2009 standard [41], where

$$DOC(\%) = \left[\frac{(H_A/H_B - 0.728)}{1.549} \right] \times 100 \qquad (1)$$

In Eq. 1, H_A is the intensity of the carbonyl linkages peak found at 1305 cm^{-1}, while H_B is the intensity of the diphenyl ether groups peak located at 1280 cm^{-1} [12].

2.2.3. Differential scanning calorimetry

The laser-heated region of the PEEK samples that are heated with 600 W and a heating duration between 1 ms and 14 ms is examined with DSC (Perkin Elmer DSC 4000) in a nitrogen atmosphere (20 ml/min). The examined specimens have a mass between 10–15 mg and are heated from 20 °C to 360 °C at a heating rate of 10 °C/min.

2.2.4. Raman spectroscopy

A number of studies have identified a correlation between the Raman spectra and the DOC of PEEK [42–49]. Doumeng et al. thoroughly examined the crystallinity of PEEK with Raman spectroscopy, density, DSC, and X-ray Diffraction (XRD). They found that Raman spectroscopy had the best correlation with the results of density, which is the most accurate method for assessing the DOC of PEEK [42]. Out of 18 examined indicators, the 1146/1595 cm^{-1} intensity ratio, and the 1644/1651 cm^{-1} intensity and area ratios agreed above 80% with the results of density, while the best correlation was achieved by the 1651 cm^{-1} band shift (92%) [42]. This band translates towards a lower wavenumber up to 10 cm^{-1} as the DOC of PEEK increases [42], which was also captured in the study of Everall et al. that similarly identified a good correlation between their Raman spectroscopy and XRD investigations (94%) [46]. Considering these findings, Raman spectroscopy could serve for assessing the crystallinity content of PEEK after laser heating. Previously, it has been used to examine its DOC after tribological tests [45], but so far it has not been applied for assessing the crystallinity changes in laser-heated PEEK. Hence, Raman spectroscopy is employed in this study and a Horiba LabRAM HR 800 confocal spectrometer is used with a 1800 lines/mm holographic grating and a helium-neon laser emitting at 633 nm. A magnification of 100× is applied at the Raman measurements with a spot diameter of 1 μm and a spectral resolution of 3 cm^{-1}. To proceed to a localised crystallinity assessment, 20 accumulations take place in each examined region for an

acquisition time of 1 s and 25% of the maximum laser power which was equal to 7.6 mW.

2.2.5. Nanoindentation

Nanoindentation is a non-destructive experimental technique that can investigate the material's mechanical properties at both the micro- and the nano-scale [50]. Since the early 2000s, it has been increasingly used to examine the properties of polymers and composites [51–56]. Especially CSM nanoindentation has increased applicability in polymer matrix composites (PMCs) [22,50–52,57]. It allows the continuous measurement of the material's hardness and contact stiffness and can also capture their variation as a function of the indentation depth. It has been employed to examine the mechanical properties of PEEK after annealing thermal treatment [39,58], and long-time heating [22], but no studies have been reported that used nanoindentation to examine the mechanical properties of laser-heated PEEK.

To do so, an Agilent G200 CSM nanoindenter equipped with a three-sided Berkovich pyramidal tip is used in this work, and the loading-unloading cycles are performed at the University of Limerick (UL), Ireland. An average of 65 ± 15 indentations take place in the thermally affected region of each sample with an indentation strain rate equal to 0.05 1/s and an indentation depth of 2000 nm. This depth ensures the validity of the method which can be highly sensitive to tip blunting, size-scale effects, and surface roughness phenomena at shallow indentation depths [54,59]. Besides the primary load, a simultaneous oscillating sinusoidal force is applied during CSM nanoindentation which in this work has a frequency of 45 Hz and an amplitude of 2 nm. Taken together, to capture the material's hardness H as a function of the indentation depth, Eq. 2 is used:

$$H = \frac{P}{A_c} \quad (2)$$

where the load of the indenter tip P is divided by the projected contact area A_c, which is calculated using the Oliver and Pharr method [60] as expressed by

$$A_c = 24.5h_c^2 + C_1 h_c^1 + C_2 h_c^{1/2} + C_3 h_c^{1/4} + \ldots + C_8 h_c^{1/128} \quad (3)$$

In Eq. 3, A_c is a function of the contact depth h_c while the constants C_1 to C_8 are obtained during the calibration process and account for any deviations that might exist between the applied and the ideal tip geometry [50,58]. CSM nanoindentation can also capture the elastic modulus E of the indented material, which is first related to the reduced modulus E_r as shown by

$$\frac{1}{E_r} = \frac{1 - \nu_s^2}{E} + \frac{1 - \nu_i^2}{i} \quad (4)$$

where E_i and ν_i are the indenter's elastic modulus and Poisson's ratio and E and ν_s are the elastic modulus and the Poisson's ratio of the sample. The reduced modulus E_r expresses the simultaneous elastic deformation of both the indenter and the indented sample and is also linked with the contact stiffness S with

$$E_r = \frac{S}{2\lambda} \sqrt{\frac{\pi}{A_c}} \quad (5)$$

where A_c is the projected contact area (Eq. 3) and λ is a correction factor proposed by Hay et al. [59] equal to 1.034 when a Berkovich tip is used [58]. In the standard nanoindentation mode, the contact stiffness S equals the slope of the unloading curve at the beginning of the unloading cycle. On the other hand, CSM nanoindentation continuously captures the deviation of S as a function of the indentation depth. This capability can prevent the depth-dependent effects that usually add incorrect bias or scatter to the unloading contact stiffness S of the polymeric materials [50] and is beneficial for measuring the properties of polymers and PMCs [50]. Altogether, to calculate the contact stiffness S with CSM

nanoindentation

$$S = \left[\frac{1}{\frac{P_0}{h_0} cos(\phi) - (K_s - m\omega^2)} - \frac{1}{K_f} \right]^{-1} \quad (6)$$

is applied, where P_0 is the oscillatory force amplitude and h_0 is the oscillatory displacement amplitude, while ω and ϕ represent the oscillation frequency and the phase angle between the load and the displacement respectively [61]. K_s and K_f are the support spring and the load frame stiffness of the instrument, and m is the mass of the indenter. In all, after combining Eq. 3, Eq. 4, Eq. 5, and Eq. 6 the elastic modulus E of the indented material is obtained with CSM nanoindentation as a function of the indentation depth.

3. Results and discussion

3.1. Optical microscopy

It is interesting to describe the damage formation pattern that is observed in laser-heated PEEK as the heating duration increases (Fig. 1). First, thermally affected regions of a small area are sporadically found on the surface of PEEK at 1 ms (Fig. 1a). Increasing the heating duration to 2 ms increases the number of these damage regions and a grainy superficial region is also formed that acts as a connecting element between them (Fig. 1b). An even further increase, results in a more uniform and coherent superficial damage region, which gets visible to the naked eye for a heating duration ≥ 4 ms (Fig. 1c - Fig. 1f). Furthermore, as expected, increasing the heating duration increases the extent of the thermally affected region on the surface of PEEK. This is shown in Fig. 2, which illustrates a global view of the samples heated with 2 ms and 6 ms. Nevertheless, the cross-sectional view of the 14 ms sample shows that even at 14 ms the heat-affected zone is close to the heated surface and the inner part remains mostly unaffected (Fig. 2c). This is attributed to the carbonaceous char layer that is formed on the surface of PEEK. Its formation is captured with ATR-FTIR that detects the occurrence of surface carbonisation at a heating duration ≥ 4 ms (Fig. 3). Finally, the observed shielding effect is corroborated by the nanoindentation results which show that the formed char layer limits the mechanical properties deterioration on the surface of the laser-heated PEEK (Section 3.5.2).

3.2. ATR-FTIR

3.2.1. Captured spectral changes and degradation mechanisms in laser-heated PEEK

The main spectral changes that occur in laser-heated PEEK are within the 1800 - 600 cm^{-1} spectral region (Fig. 3) and a detailed description can be found in Table 1. In Fig. 3, the first two arrows at 1711 cm^{-1} and at 1452 cm^{-1} indicate the formation of a new fluorenone peak. Recently, its intensity has been correlated with the extent of thermal degradation that occurs in PEEK and CF/PEEK after rapid high-temperature processing [26], and its development in laser-heated PEEK is also indicative of thermal degradation (Fig. 3). The changes in the 1305/1280 cm^{-1} and 966/952 cm^{-1} intensity ratios demonstrate changes in the crystallinity content of PEEK [33,62], and the detected shoulder at 1253 cm^{-1} and the variations around 1110 cm^{-1} show that chain scission and crosslinking mechanisms take place [27,63] (Fig. 3, Table 1). Finally, the reduction in the aromatic C-H peaks around 835 cm^{-1}, 766 cm^{-1} and 673 cm^{-1} highlights the occurrence of surface carbonisation in the laser-heated samples [12], which agrees with the OM results where a char layer is captured for a heating duration ≥ 4 ms (Fig. 1).

Altogether, ATR-FTIR detects chain scission, crosslinking mechanisms, and surface carbonisation on the surface of laser-heated PEEK, and the observed spectral changes are found more significant as the heating duration increases (Fig. 3). These spectral changes are first
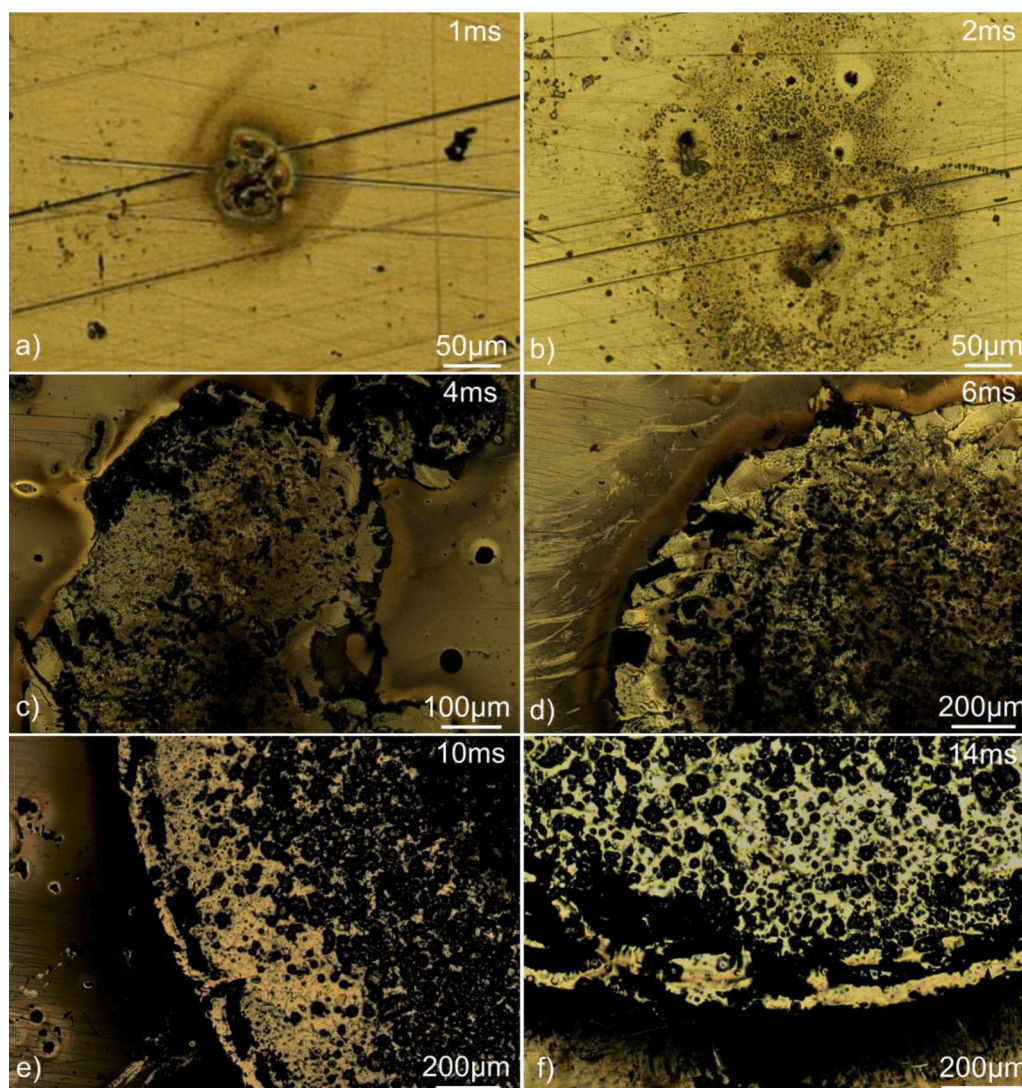
Fig. 1. Thermal damage on the surface of PEEK, when laser heated with a Gaussian beam of a 5 mm diameter, a power of 600 W, and a heating duration of a) 1 ms, b) 2 ms, c) 4 ms, d) 6 ms, e) 10 ms, and f) 14 ms.

noticed in the 4 ms sample, while the spectra of the samples heated for 1 ms and 2 ms are similar to the spectra of the as-received PEEK. This is because ATR-FTIR examines a wider surface, and therefore - being governed by scale-related issues - it cannot detect the occurrence of thermal degradation despite the small area thermal damage induced (Fig. 1a, Fig. 1b). To address this issue, localised measurements with micro-FTIR or Raman spectroscopy are recommended and Raman spectroscopy is applied in this study to assess the surface of these samples (Section 3.4.2).

3.2.2. The degree of crystallinity in laser-heated PEEK after capturing the $1305/1280\,cm^{-1}$ intensity ratio

To investigate the effect of laser heating on the DOC of PEEK, the intensity ratio of the $1305/1280\,cm^{-1}$ IR bands is examined, and a decrease is noticed in the samples heated for a heating duration ≥ 4 ms compared to virgin PEEK (Fig. 4). Opposite to that, the 1 ms and 2 ms samples show a slight increase in their $1305/1280\,cm^{-1}$ intensity ratios (Table 2). These findings indicate a more significant crystalline morphology in the samples heated for 1 ms and 2 ms, and a reduced crystallinity content for a duration ≥ 4 ms compared to virgin PEEK [33]. This is clearly shown in Fig. 4c, where the DOC of PEEK is calculated after applying Eq. 1. The captured DOC increase at 1 ms and 2 ms is attributed to recrystallisation phenomena that take place [28], which

shows that short-time laser heating operates as an annealing process when the reached temperatures surpass the material's T_g but do not yet reach the onset of thermal degradation. A further increase in the heating duration (≥ 4 ms) triggers the degradation mechanisms and leads to surface carbonisation (Fig. 1, Fig. 3). This significantly impacts the crystallinity of PEEK which reaches a plateau of around 11% (Fig. 4). Consequently, the analysis shows that surface carbonisation is associated with the thermal limits of laser-heated PEEK, and its detection with ATR-FTIR could be a quick method for identifying the critical processing conditions of PEEK in laser heating.

3.3. Differential scanning calorimetry

The DSC thermograms of the laser-heated PEEK samples are found similar to that of virgin PEEK and significant changes are not identified (Fig. 5). A slight increase is mainly noted in the T_m of PEEK with the applied laser heating. Likewise, the area under the endothermic melting peak is in a range of similar values which indicates that the DOC of PEEK has not been affected by the applied laser heating (Fig. 5). Nonetheless, the whole sample's thickness is examined with DSC and thus both heat-affected region and bulk material are examined. Therefore, since the resulting thermal damage is mostly superficial (Fig. 2c) DSC inevitably neglects it. This is the main reason that this method cannot capture
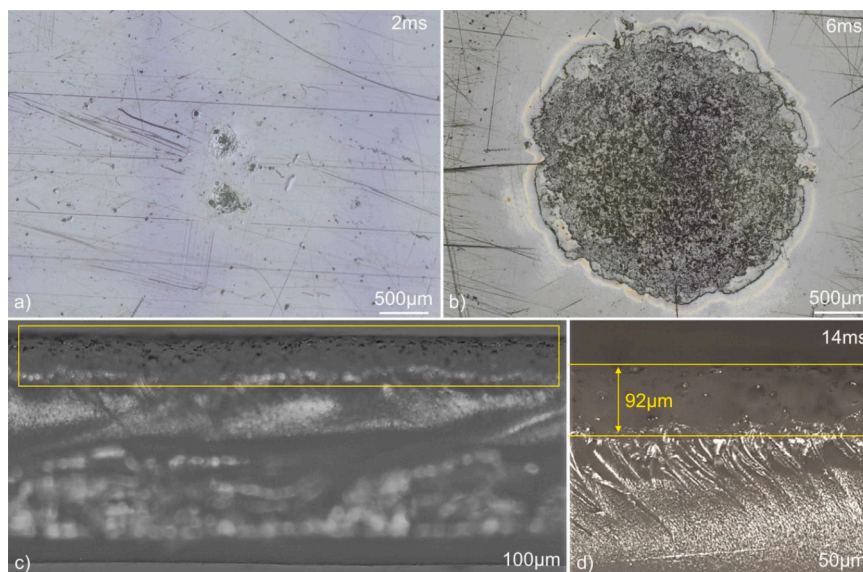
Fig. 2. Global view of the thermal damage on the surface of PEEK when laser heated with a) 2 ms, and b) 6 ms & thermal damage in the through-thickness direction of the sample heated with 14 ms: c) global view, and d) detail.
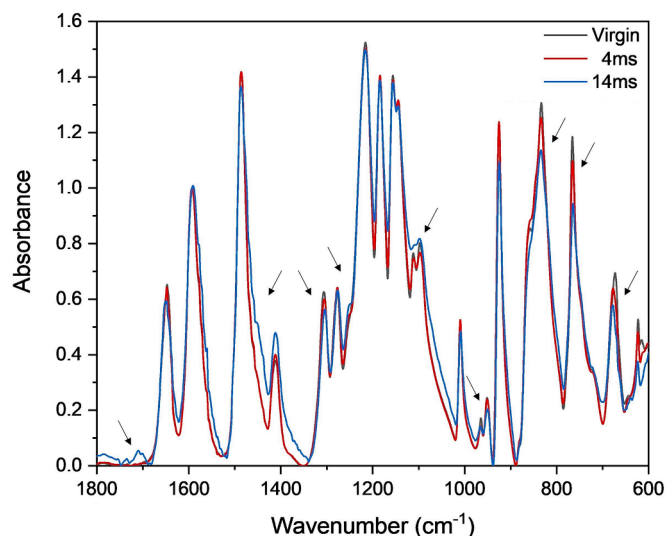

Fig. 3. IR spectra of virgin and laser-heated PEEK with a Gaussian beam of a 5 mm diameter, a power of 600 W, and a heating duration of 4 ms and 14 ms.

significant changes in the laser-heated PEEK samples of this study. To counteract this issue, micro-cutting methods should be employed that would allow the individual evaluation of the thermally affected region. Nevertheless, a cold crystallisation peak is found at around 175 °C,

despite the underpinning scale-related issues. This peak indicates an increased amorphous content in the laser-heated PEEK samples, which - after going through a recrystallisation process during the DSC runs - results in the formed cold crystallisation peak (Fig. 5). It starts developing at 4 ms and it is clearly evident when a heating duration $\geq$ 6 ms is applied (Fig. 5). Interestingly, these findings agree with the OM investigation that captures coherent thermal damage at 4 ms (Fig. 1c), and significant thermal damage for a heating duration $\geq$ 6 ms (Fig. 1d - Fig. 1f).

3.4. Raman spectroscopy

3.4.1. Changes in the Raman spectra of PEEK upon laser heating

In Fig. 6, the Raman spectra of virgin PEEK and of the laser-heated PEEK samples for 4 ms and 14 ms are presented. The strongest peak in the 1100 - 1700 cm^{-1} region is at 1146 cm^{-1} which is associated with the C–O–C stretching mode of PEEK, while the weakest peak is at 1202 cm^{-1} that is assigned to its anti-symmetric C–O–C stretching mode [47]. The characteristic peaks at 1595 cm^{-1} and 1608 cm^{-1} correspond to the phenyl ring vibrations, while the 1644 cm^{-1} band is assigned to the C==O stretching [47]. Several research groups have divided the 1644 cm^{-1} peak into two different bands at 1644 cm^{-1} and 1651 cm^{-1}, which correspond to the C==O stretching of the crystalline and of the amorphous PEEK respectively [42–45]. Considering that the strongest peak at 1146 cm^{-1} is strongly related to changes in crystallinity, the second strongest peak at 1595 cm^{-1} peak is used as the normalisation reference in this analysis [45] and three main changes are identified in

Table 1

Spectral changes noted at PEEK after laser heating with a Gaussian beam of a 5 mm diameter, a power of 600 W, and a heating duration up to 14 ms.

| Wavenumber (cm^{-1})	Observed spectral changes upon short-time laser heating (1800 - 600 cm^{-1})
1711, 1452	Formation of a new fluorenone peak
1305, 1280	Changes in the intensity ratio of the two bands (indicative of changes in crystallinity)
1253	Growth of a shoulder in the high-frequency side of the ether peak at 1216 cm^{-1}
1100	Changes in the diphenylether bonds
966, 951	Changes in the intensity ratio of the two bands (indicative of changes in crystallinity)
863, 835, 766, 673	Changes in the aromatic rings
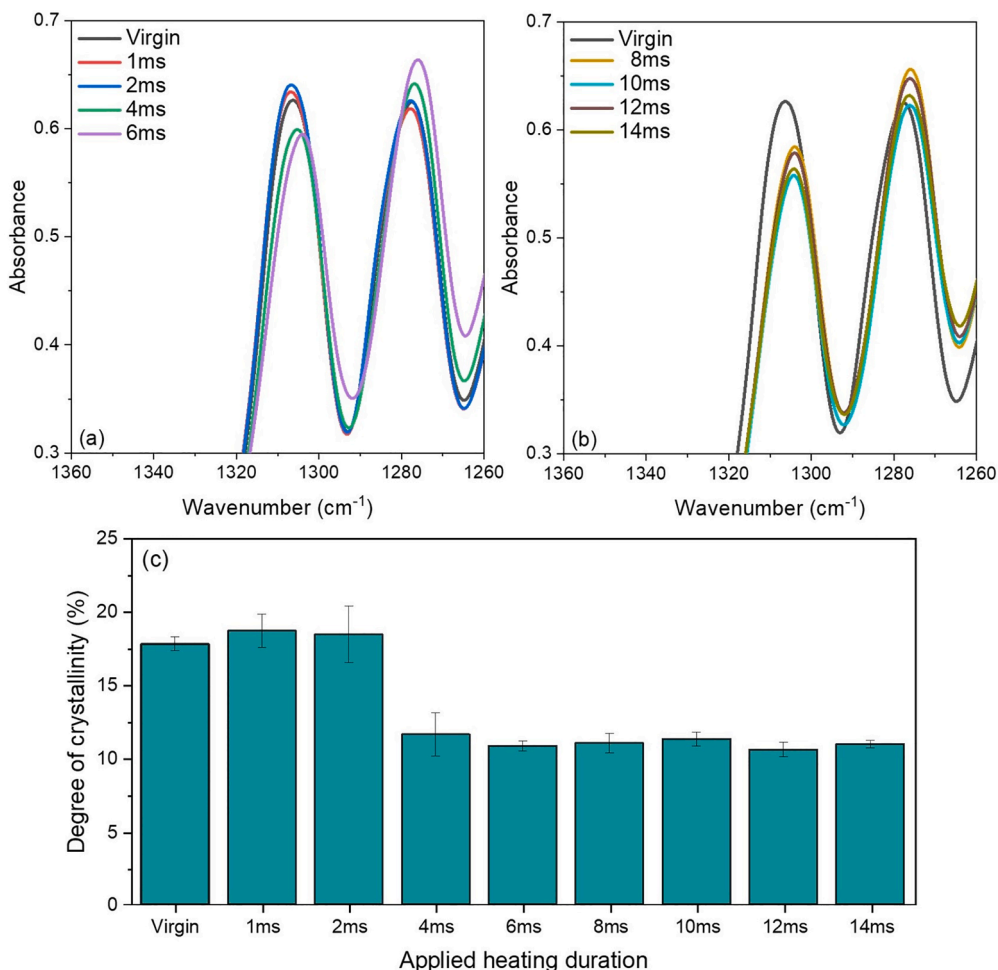
Fig. 4. IR spectra of virgin and laser-heated PEEK with a Gaussian beam of a 5 mm diameter, a power of 600 W, and a heating duration up to 14 ms: a,b) 1305 cm^{-1}, 1280 cm^{-1} & c) degree of crystallinity (average value and standard deviation).
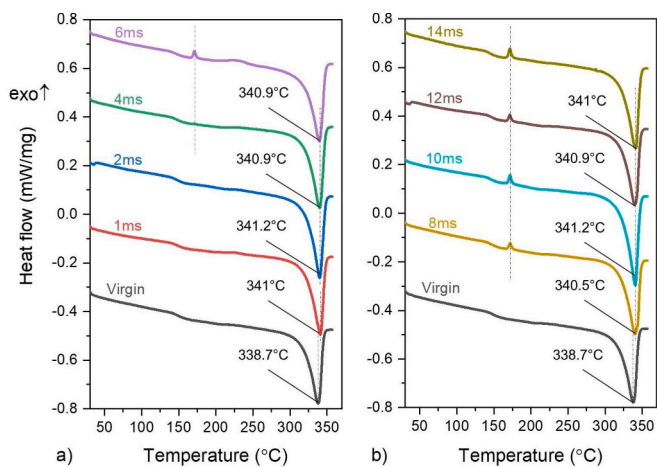

Fig. 5. DSC thermograms of virgin and laser-heated PEEK with a Gaussian beam of a 5 mm diameter, a power of 600 W, and a heating duration up to 14 ms.
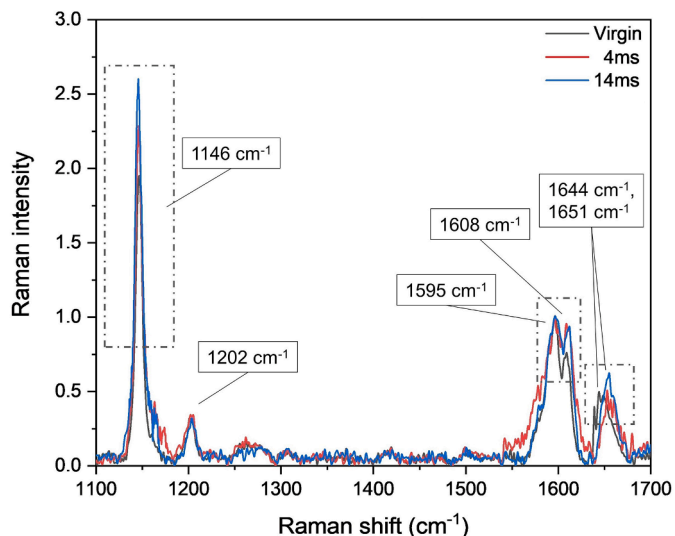

Fig. 6. Raman spectra of virgin and laser-heated PEEK with a Gaussian beam of a 5 mm diameter, a power of 600 W, and a heating duration of 4 ms and 14 ms.

the Raman spectra of PEEK upon laser heating (Fig. 6).

First, the C==O stretching peak shifts from 1644 cm^{-1} at the virgin material towards 1653 cm^{-1} and 1655 cm^{-1} at the samples heated for 4 ms and 14 ms respectively. These wavenumbers are associated with the amorphous region of PEEK, which shows that the applied laser heating

reduces the crystallinity content on its surface [42,46], with a higher reduction at the sample heated for 14 ms (1655 cm^{-1}). Likewise, the decrease in the 1595/1608 cm^{-1} intensity ratio is also representative of
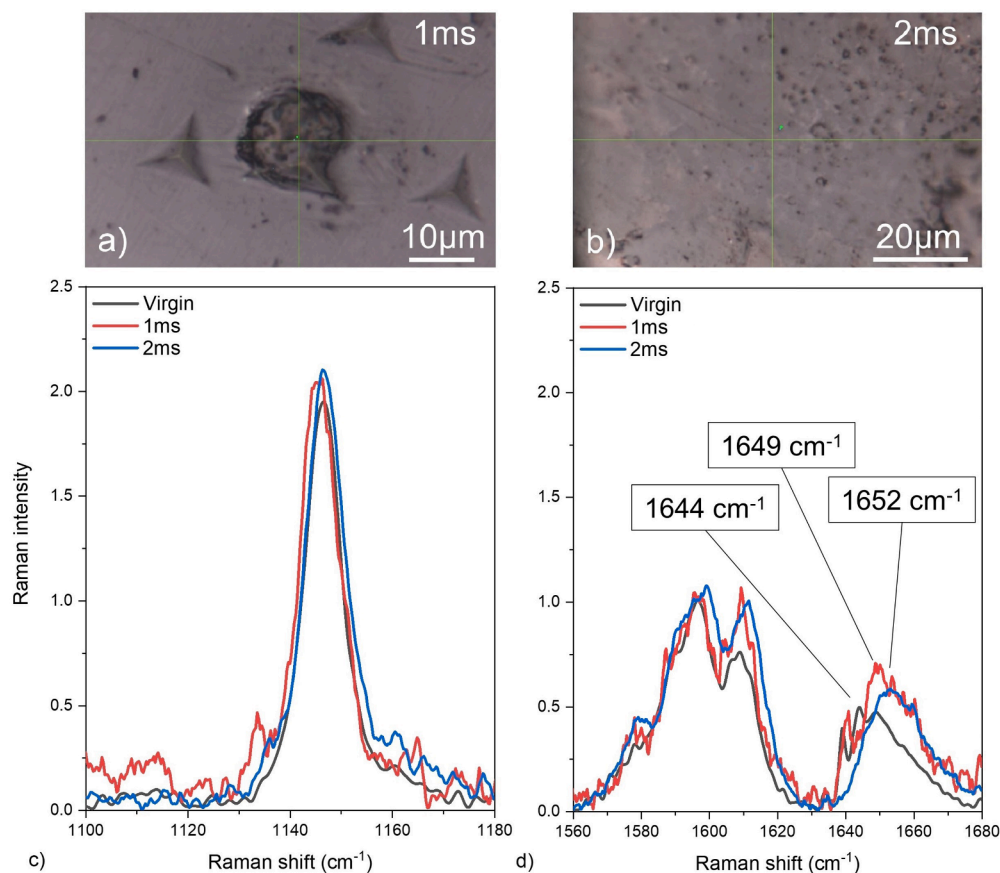
Fig. 7. Localised Raman measurements in the small-area thermal damage of the laser-heated PEEK samples with a Gaussian beam of a 5 mm diameter, a power of 600 W, and a heating duration of a) 1 ms, and b) 2 ms & their corresponding Raman spectra: c) $1146/1595$ cm^{-1} intensity ratio, d) 1644 cm^{-1} band shift.

a lower crystallinity content in the laser-heated samples [42,43,48,49], and this is also the case with the observed increase in the $1146/1595$ cm^{-1} intensity ratio, which is also stronger in the 14 ms sample (Fig. 6) [42,49,64]. Notably, these results agree with the ATR-FTIR analysis, where the intensity ratio of the $1305/1280$ cm^{-1} IR bands also captured a decrease in the DOC of PEEK after the applied laser heating of 4 ms and 14 ms.

3.4.2. Using Raman spectroscopy to locally assess the small-area thermal damage of laser-heated PEEK

Fig. 7 presents the localised measurements that take place with Raman spectroscopy for assessing the thermally affected region of the PEEK samples heated for 1 ms and 2 ms. In these samples, a small-area thermal damage is induced with the applied laser heating (Fig. 1) that cannot be evaluated with ATR-FTIR or DSC due to scale-related issues. Therefore, to proceed to a valid crystallinity assessment Raman spectroscopy is applied and the 1651 cm^{-1} band shift and the $1146/1595$ cm^{-1} intensity ratio are examined (Fig. 7c, Fig. 7d). Similarly to Fig. 6, a slight increase in the $1146/1595$ cm^{-1} intensity ratio is identified at the samples heated for 1 ms and 2 ms compared to virgin PEEK (Fig. 7c). Furthermore, the C==O stretching peak shifts from 1644 cm^{-1} towards 1649 cm^{-1} and 1652 cm^{-1} (Fig. 7d). These changes show a decrease in the crystallinity content of PEEK in the small-area thermal damage of these samples. Taken together, opposite to ATR-FTIR and DSC, Raman spectroscopy is suitable for assessing the crystallinity content of PEEK in cases where small-area thermal damage is induced. This is one of the main benefits of this approach, especially in applications where laser heating is involved and the processing conditions that would activate the thermal degradation mechanisms of PEEK cannot be easily defined. Raman spectroscopy could be a significant tool in these

applications for further assessing the thermal limits of PEEK.

3.5. Nanoindentation

3.5.1. Properties of virgin (as-received) PEEK and applied methodology

Similarly to Raman spectroscopy, nanoindentation can carry localised measurements on the surface of PEEK and is suitable for examining the mechanical properties of the laser-heated samples. It can be effectively used for assessing the small-area thermal damage in the 1 ms and 2 ms samples and it can also accurately assess the more significant and coherent thermal damage that occurs in PEEK for a longer heating duration (Fig. 1). First, to derive the properties of virgin PEEK three samples are examined and 120 indentations take place on their examined regions. Fig. 8 illustrates the hardness and the indentation modulus of the virgin (as-received) PEEK as a function of the indentation depth and the analysis captures an average hardness of 0.28 GPa $\pm$ 0.03 GPa and an average indentation modulus of 3.98 GPa $\pm$ 0.28 GPa. After assessing the properties of the as-received PEEK, the effect of the applied laser heating on its mechanical properties is examined. Each sample is tested with an average of 65 indentations, and to illustrate the process, examples of indented locations are presented in Fig. 9. Overall, to capture the most significant thermal effect on each sample, localised measurements around the thermally induced damage take place.

3.5.2. The shielding mechanism of the char layer

Fig. 10 displays the average hardness and indentation modulus of the samples heated for 1 ms and 12 ms together with the properties of virgin PEEK. The 12 ms sample is severely affected at shallow indentation depths (close to the surface), while both its hardness and indentation modulus increase as the indentation depth increases. For example, the
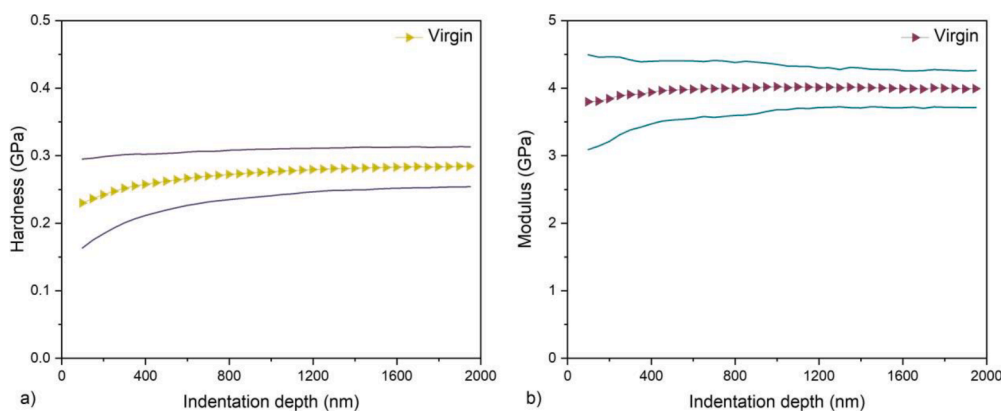
Fig. 8. a) Hardness and b) indentation modulus of the virgin (as-received) PEEK as a function of the indentation depth (average values and standard deviation).
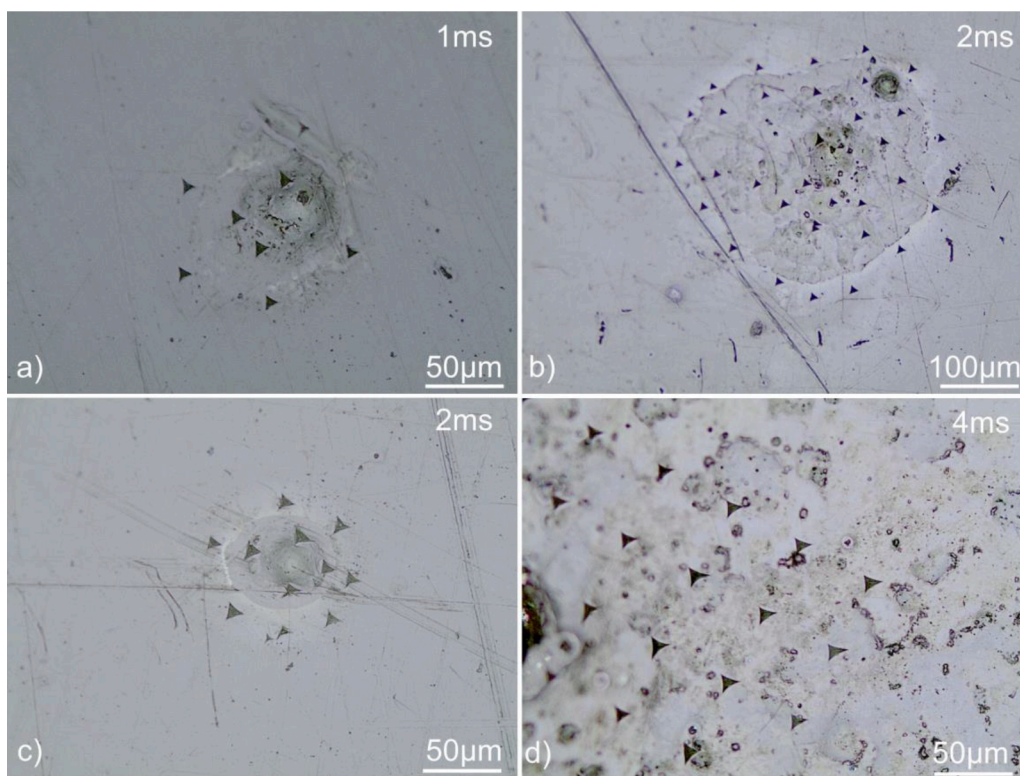

Fig. 9. Examples of indented locations at the thermally affected area of the laser-heated PEEK samples with a Gaussian beam of a 5 mm diameter, a power of 600 W, and a heating duration of a) 1 ms, b-c) 2 ms, and d) 4 ms.

indentation modulus is approximately 34% of the modulus of virgin PEEK at 100 nm and it has already reached 76% at 1950 nm (3.05 GPa) (Fig. 10b). This behaviour is evident in all the PEEK samples that are laser heated for a duration ≥ 4 ms (Fig. 13). As shown with OM and ATR-FTIR, surface carbonisation takes place in these samples, and a char layer is formed. This char layer is the main reason that the induced thermal damage is mostly found on the surface of PEEK. For example, previous studies have shown that it acts as a protective layer during the decomposition of PEEK that limits the access of heat to the bulk material [23,27,65]. As a matter of fact, Fig. 10 shows that the properties of the laser-heated PEEK approach the properties of the virgin PEEK in the through-thickness direction. Therefore, the nanoindentation results show that the formed char layer "shields" the bulk PEEK from the consequences of the applied laser heating and results in mostly superficial thermally induced damage.

3.5.3. The hardening effect of short-time laser heating

Another interesting finding in Fig. 10 is that the applied laser heating for 1 ms improves the hardness of PEEK compared to the virgin material. This increase is up to 10.8% at an indentation depth of 500 nm (Fig. 10a), and to further examine this effect, Fig. 11 presents localised indentations at a small-area thermal damage of the 1 ms sample. As in Fig. 10, the indented location in the centre of the thermally induced damage is severely affected at shallow indentation depths, while both its hardness and indentation modulus increase as the indentation depth increases (Fig. 11c, Fig. 11d). Interestingly, the results in the surrounding area show a different response with a notable increase taking place in the average hardness of the region and an average indentation modulus similar to that of virgin PEEK. Hence, a hardening effect takes place in the area surrounding the thermally induced damage of the 1 ms sample (Fig. 11c). Similarly to the captured crystallinity increase in Fig. 4c, this hardening effect is attributed to the recrystallisation that
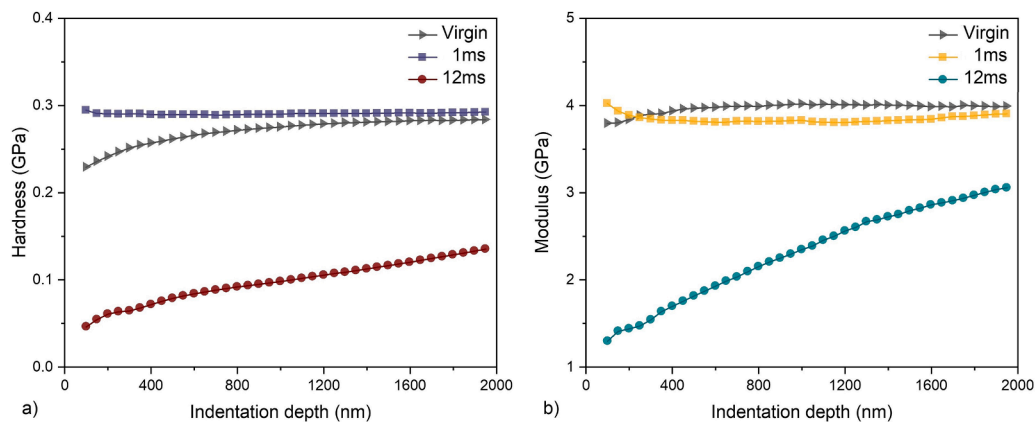
Fig. 10. a) Hardness, and b) indentation modulus of virgin and laser-heated PEEK with a Gaussian beam of a 5 mm diameter, a power of 600 W, and a heating duration of 1 ms, and 12 ms as a function of the indentation depth (average values).
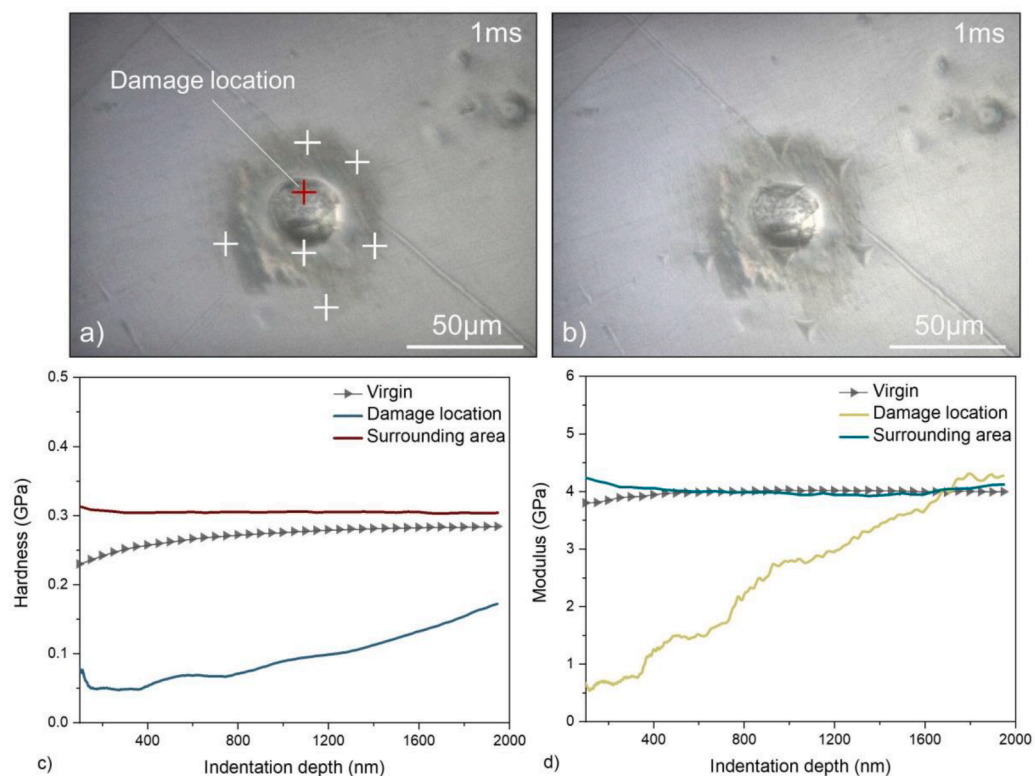

Fig. 11. Indented locations (600 W - 1 ms) a) before, and b) after the test & c) hardness, and d) indentation modulus as a function of the indentation depth at the damage location, and at the surrounding area (average values).

takes place on the surface of PEEK upon the applied short-time laser heating.

In summary, both nanoindentation and ATR-FTIR demonstrate that short-time laser heating mostly functions as an annealing process when a heating duration equal to 1 ms is applied. This is an interesting finding and shows that short-time laser heating could be used as a tailoring mechanism in laser applications of PEEK. For example, in the aerospace industry a laser repass treatment is commonly applied to CF/PEEK structures manufactured with LATP [10,66]. This takes place mostly for assisting with thermal stress relief and cold crystallization phenomena [10]. Furthermore, short-time laser heating could potentially also be used to influence properties of the bulk composite such as the inter-laminar shear strength (ILSS), which is currently extensively researched in LATP applications of CF/PEEK [8–10,67].

3.5.4. Concluding remarks on the nanoindentation of laser-heated PEEK
Fig. 12 and Fig. 13 present the hardness and modulus of the laser-heated PEEK samples at an indentation depth of 500 nm, 1000 nm, and 1500 nm. These figures illustrate the main findings of this investigation and provide important information about the response of PEEK when it is laser heated for an increasing heating duration. Overall, two distinct groups of samples can be identified in the examined case study which show a different response.

Initially, in the samples heated for a duration $\geq$ 4 ms surface carbonisation occurs and a char layer is formed (Fig. 1, Fig. 3). These phenomena significantly affect their mechanical properties and result in a decrease of around 50% and 45% in their hardness and indentation modulus respectively (Fig. 12, Fig. 13). However, similar hardness and moduli values are found amongst these samples which demonstrates
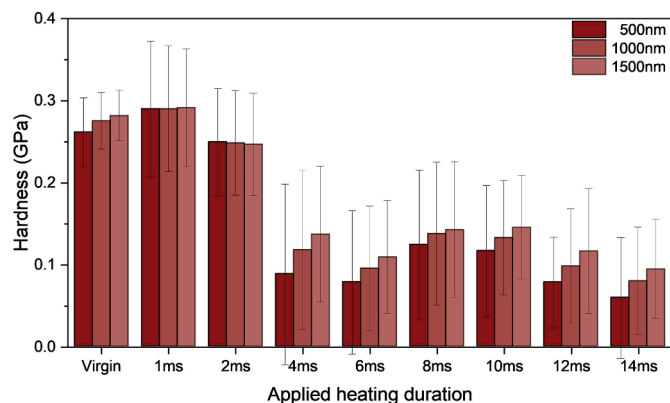
Fig. 12. Hardness at a depth of 500 nm, 1000 nm, and 1500 nm of virgin and laser-heated PEEK with a Gaussian beam of a 5 mm diameter, a power of 600 W, and a heating duration up to 14 ms.
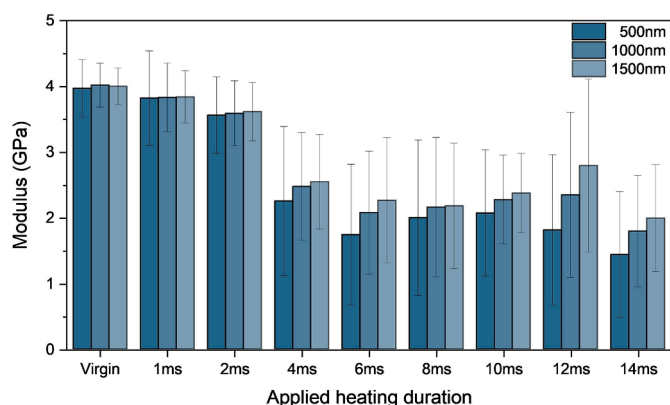

Fig. 13. Indentation modulus at a depth of 500 nm, 1000 nm, and 1500 nm of virgin and laser-heated PEEK with a Gaussian beam of a 5 mm diameter, a power of 600 W, and a heating duration up to 14 ms.

that after the formation of the char layer the material is not further affected by the increase in the applied heating duration. The analysis also shows that the most significant damage takes place at shallow depths and the material properties increase as the indentation depth increases. This increase is sharper in the heated samples compared to virgin PEEK and is attributed to the shielding mechanism of the formed char layer that limits the access of heat to the bulk PEEK. Therefore, the formed char layer constrains the damage close to the heated surface, thus securing the mechanical properties of PEEK in its through-thickness direction.

On the other hand, the samples heated for 1 ms and 2 ms show a

different response. Especially at the 1 ms sample, an increase is observed in its hardness while the moduli of both samples slightly decrease. Moreover, significant variations do not occur with the indentation depth which also differs from the captured behaviour in virgin PEEK and in the samples heated for $\geq$ 4 ms (Fig. 12, Fig. 13). As discussed in the ATR-FTIR analysis, a higher DOC is found on the surface of these samples compared to virgin PEEK (Fig. 4). This is attributed to the recrystallisation phenomena that take place in these conditions, which also result in the observed hardening effect (Fig. 11). Hence, besides triggering the thermal degradation mechanisms in a few locations, short-time laser heating mostly operates as an annealing process that triggers recrystallisation and hardening phenomena on the surface of PEEK thus improving its superficial properties. Taken together, to conclude the analysis Table 2 gathers the main results of ATR-FTIR and nanoindentation.

4. Conclusions

In the present work, the response of PEEK subject to laser heating was examined and the applicability of various experimental methods in assessing the thermal degradation of laser-heated PEEK was investigated. The analysis shows that two main mechanisms take place on the surface of PEEK upon laser heating and the main conclusions are the following:

- Short-time laser heating acts as an annealing process that triggers recrystallisation and hardening phenomena that increase the crystallinity and the hardness on the surface of PEEK by up to 5.1% and 10.8% respectively.
- A further increase in the heating duration results in surface carbonisation and char layer formation. These phenomena significantly decrease the DOC of PEEK by up to 41%. They also reduce its hardness, and indentation modulus by around 50%, and 45% respectively.
- Surface carbonisation is associated with the thermal limits of PEEK in laser heating, and its detection with ATR-FTIR can serve as a quick method for defining its optimum process window in laser applications.
- The char layer acts as a protective layer that limits the access of heat to the bulk PEEK, restricting the severe thermal damage on its surface and shielding the bulk material from the applied thermal load.
- Nanoindentation and Raman spectroscopy are suitable for identifying the laser processing that would act as an annealing process, and they can be useful techniques for studies that aim to identify the optimum laser processing of PEEK.

In summary, the conducted multi-technique experimental analysis thoroughly examined the thermal degradation mechanisms of laser-heated PEEK, and it identified suitable degradation detection techniques for laser heating of polymers and PMCs. The findings could be

Table 2
Main outputs of the ATR-FTIR and nanoindentation analysis.

Heating duration	1305/1280 cm^{-1} IR intensity ratio	DOC (Eq. 1) (%)	Hardness at 1500 nm (GPa)	Modulus at 1500 nm (GPa)
Virgin (0 ms)	1.003 ± 0.007	17.72 ± 0.47	0.282 ± 0.031	3.999 ± 0.279
1 ms	1.016 ± 0.017	18.62 ± 1.12	0.291 ± 0.072	3.836 ± 0.398
2 ms	1.013 ± 0.030	18.38 ± 1.94	0.246 ± 0.062	3.614 ± 0.444
4 ms	0.943 ± 0.064	11.56 ± 1.46	0.137 ± 0.083	2.546 ± 0.720
6 ms	0.895 ± 0.005	10.77 ± 0.32	0.109 ± 0.069	2.266 ± 0.953
8 ms	0.892 ± 0.014	10.97 ± 0.65	0.142 ± 0.083	2.181 ± 0.953
10 ms	0.910 ± 0.022	11.25 ± 0.48	0.145 ± 0.063	2.376 ± 0.602
12 ms	0.891 ± 0.008	10.53 ± 0.49	0.116 ± 0.077	2.793 ± 1.317
14 ms	0.897 ± 0.004	10.90 ± 0.24	0.094 ± 0.060	1.994 ± 0.813

relevant for studies that aim to identify the optimum laser heating of PEEK that would positively affect the material without inducing significant thermal damage on its surface. By doing so, short-time laser heating could be used for tailoring the properties on the surface of PEEK in a desired manner. For example, it could serve for increasing the material's crystallinity or roughness, thus further enhancing the implementation of PEEK in several industrial applications where laser heating is involved, such as laser-assisted tape placement (LATP) applications in the aerospace industry or medical applications.

CRediT authorship contribution statement

Dimitrios Gaitanelis: Conceptualization, Methodology, Validation, Formal analysis, Investigation, Data curation, Writing – original draft, Writing – review & editing, Visualization. **Angeliki Chanteli:** Conceptualization, Investigation, Writing – review & editing, Visualization. **Chris Worrall:** Conceptualization, Supervision, Project administration, Resources, Writing – review & editing. **Paul M. Weaver:** Conceptualization, Supervision, Project administration, Resources, Writing – review & editing. **Mihalis Kazilas:** Conceptualization, Supervision, Project administration, Resources, Writing – review & editing, Funding acquisition.

Declaration of Competing Interest

The authors declare that they have no known competing financial interests or personal relationships that could have appeared to influence the work reported in this paper.

Data availability

Data will be made available on request.

Acknowledgement

References

[1] M. Martn, F. Rodrguez-Lence, A. Gemes, A. Fernndez-Lpez, L. Prez-Maqueda, A. Perejn, On the determination of thermal degradation effects and detection techniques for thermoplastic composites obtained by automatic lamination, Composites Part A: Applied Science and Manufacturing 111 (2018) 23–32, https://doi.org/10.1016/j.compositesa.2018.05.006.

[2] G. Dolo, J. Frec, D. Carti, Y. Grohens, G. Ausias, Model for thermal degradation of carbon fiber filled poly(ether ether ketone), Polym. Degrad. Stab. 143 (2017) 20–25, https://doi.org/10.1016/j.polymdegradstab.2017.06.006.

[3] C. Stokes-Griffin, P. Compston, An inverse model for optimisation of laser heat flux distributions in an automated laser tape placement process for carbon-fibre/PEEK, Composites Part A: Applied Science and Manufacturing 88 (2016) 190–197, https://doi.org/10.1016/j.compositesa.2016.05.034.

[4] C. Tan, J. Su, B. Zhu, X. Li, L. Wu, B. Chen, X. Song, J. Feng, Effect of scanning speed on laser joining of carbon fiber reinforced PEEK to titanium alloy, Optics & Laser Technology 129 (2020) 106273, https://doi.org/10.1016/j.optlastec.2020.106273.

[5] C. Leone, S. Genna, Heat affected zone extension in pulsed ND:YAG laser cutting of CFRP, Composites Part B: Engineering 140 (2018) 174–182, https://doi.org/10.1016/j.compositesb.2017.12.028.

[6] D. Peeters, G. Clancy, V. Oliveri, R. O'Higgins, D. Jones, P.M. Weaver, Concurrent design and manufacture of a thermoplastic composite stiffener, Compos Struct 212 (2019) 271–280, https://doi.org/10.1016/j.compstruct.2019.01.033.

[7] A.K. Bandaru, G.J. Clancy, D. Peeters, R. O'Higgins, P.M. Weaver, Interface Characterization of Thermoplastic Skin-Stiffener Composite Manufactured using Laser-Assisted Tape Placement, ???? 10.2514/6.2018-0481.

[8] A.K. Bandaru, G. Clancy, D. Peeters, R.M. O'Higgins, P.M. Weaver, Properties of a thermoplastic composite skin-stiffener interface in a stiffened structure manufactured by laser-assisted tape placement with in situ consolidation, Compos Struct 214 (2019) 123–131, https://doi.org/10.1016/j.compstruct.2019.02.011.

[9] C. Stokes-Griffin, P. Compston, The effect of processing temperature and placement rate on the short beam strength of carbon fibre-PEEK manufactured using a laser tape placement process, Composites Part A: Applied Science and Manufacturing 78 (2015) 274–283, https://doi.org/10.1016/j.compositesa.2015.08.008.

[10] A. Chanteli, A.K. Bandaru, D. Peeters, R.M. O'Higgins, P.M. Weaver, Influence of repass treatment on carbon fibre-reinforced PEEK composites manufactured using laser-assisted automatic tape placement, Compos Struct 248 (2020) 112539, https://doi.org/10.1016/j.compstruct.2020.112539.

[11] A. Comer, D. Ray, W. Obande, D. Jones, J. Lyons, I. Rosca, R. O'Higgins, M. McCarthy, Mechanical characterisation of carbon fibre-PEEK manufactured by laser-assisted automated-tape-placement and autoclave, Composites Part A: Applied Science and Manufacturing 69 (2015) 10–20, https://doi.org/10.1016/j.compositesa.2014.10.003.

[12] B. Cheng, H. Duan, Q. Chen, H. Shang, Y. Zhang, J. Li, T. Shao, Effect of laser treatment on the tribological performance of polyetheretherketone (PEEK) under seawater lubrication, Appl Surf Sci 566 (2021) 150668, https://doi.org/10.1016/j.apsusc.2021.150668.

[13] A. Obilor, M. Pacella, A. Wilson, V. Silberschmidt, Micro-texturing of polymer surfaces using lasers: A review, The International Journal of Advanced Manufacturing Technology 120 (2022) 103–135, https://doi.org/10.1007/s00170-022-08731-1.

[14] A. Riveiro, R. Soto, R. Comesaa, M. Boutinguiza, J. del Val, F. Quintero, F. Lusquios, J. Pou, Laser surface modification of PEEK, Appl Surf Sci 258 (23) (2012) 9437–9442, https://doi.org/10.1016/j.apsusc.2012.01.154.EMRS 2011 Spring Symp J: Laser Materials Processing for Micro and Nano Applications

[15] C. Akkan, M. Hammadeh, S. Brck, H. Park, M. Veith, H. Abdul-Khaliq, C. Aktas, Plasma and short pulse laser treatment of medical grade PEEK surfaces for controlled wetting, Mater Lett 109 (2013) 261–264, https://doi.org/10.1016/j.matlet.2013.07.030.

[16] A. Riveiro, A.L.B. Maon, J. del Val, R. Comesaa, J. Pou, Laser surface texturing of polymers for biomedical applications, Front Phys 6 (2018), https://doi.org/10.3389/fphy.2018.00016.

[17] M. Omrani, A. Hadjizadeh, A. Milani, K. Keekyoung, PEEK Surface modification methods and effect of the laser method on surface properties, Biointerface Research in Applied Chemistry 10 (2) (2020) 5132–5140, https://doi.org/10.33263/BRIAC102.132140.

[18] B. Henriques, D. Fabris, J. Mesquita-Guimares, A.C. Sousa, N. Hammes, J.C. Souza, F.S. Silva, M.C. Fredel, Influence of laser structuring of PEEK, PEEK-GF30 and PEEK-CF30 surfaces on the shear bond strength to a resin cement, J Mech Behav Biomed Mater 84 (2018) 225–234, https://doi.org/10.1016/j.jmbbm.2018.05.008.

[19] P. Laurens, B. Sadras, F. Decobert, F. Arefi-Khonsari, J. Amouroux, Enhancement of the adhesive bonding properties of PEEK by excimer laser treatment, Int. J. Adhes. Adhes. 18 (1) (1998) 19–27, https://doi.org/10.1016/S0143-7496(97)00063-8.

[20] A. Wilson, I. Jones, F. Salamat-Zadeh, J.F. Watts, Laser surface modification of poly (etheretherketone) to enhance surface free energy, wettability and adhesion, Int. J. Adhes. Adhes. 62 (2015) 69–77, https://doi.org/10.1016/j.ijadhadh.2015.06.005.

[21] V. Myllri, T.-P. Ruoko, J. Vuorinen, H. Lemmetyinen, Characterization of thermally aged polyetheretherketone fibres - mechanical, thermal, rheological and chemical property changes, Polym. Degrad. Stab. 120 (2015) 419–426, https://doi.org/10.1016/j.polymdegradstab.2015.08.003.

[22] E. Courvoisier, Y. Bicaba, X. Colin, Multi-scale and multi-technique analysis of the thermal degradation of poly(ether ether ketone), Polym. Degrad. Stab. 151 (2018) 65–79, https://doi.org/10.1016/j.polymdegradstab.2018.03.001.

[23] P. Patel, T.R. Hull, R.E. Lyon, S.I. Stoliarov, R.N. Walters, S. Crowley, N. Safronava, Investigation of the thermal decomposition and flammability of PEEK and its carbon and glass-fibre composites, Polym. Degrad. Stab. 96 (1) (2011) 12–22, https://doi.org/10.1016/j.polymdegradstab.2010.11.009.

[24] M. Day, J.D. Cooney, D.M. Wiles, The kinetics of the oxidative degradation of poly (aryl-ether-ether-ketone) (PEEK), Thermochim Acta 147 (1) (1989) 189–197, https://doi.org/10.1016/0040-6031(89)85174-3.

[25] M. Day, J.D. Cooney, D.M. Wiles, A kinetic study of the thermal decomposition of poly(aryl-ether-ether-ketone) (PEEK) in nitrogen, Polymer Engineering & Science 29 (1) (1989) 19–22, https://doi.org/10.1002/pen.760290105.

[26] D. Gaitanelis, C. Worrall, M. Kazilas, Detecting, characterising and assessing PEEK's and CF-PEEK's thermal degradation in rapid high-temperature processing, Polym. Degrad. Stab. 204 (2022) 110096, https://doi.org/10.1016/j.polymdegradstab.2022.110096.

[27] A. Pascual, M. Toma, P. Tsotra, M.C. Grob, On the stability of PEEK for short processing cycles at high temperatures and oxygen-containing atmosphere, Polym. Degrad. Stab. 165 (2019) 161–169, https://doi.org/10.1016/j.polymdegradstab.2019.04.025.

[28] S.-J. Fang, R. Salovey, S.D. Allen, Laser annealing of polyetheretherketone (PEEK), Polymer Engineering & Science 29 (18) (1989) 1241–1245, https://doi.org/10.1002/pen.760291806.

[29] T. Bayerl, M. Brzeski, M. Martnez-Tafalla, R. Schledjewski, P. Mitschang, Thermal degradation analysis of short-time heated polymers, J. Thermoplast. Compos. Mater. 28 (3) (2015) 390–414, https://doi.org/10.1177/0892705713486122.

[30] K.E. Supan, C. Robert, M.J. Miller, J.M. Warrender, F. Stephen, Thermal degradation of MWCNT/polypropylene nanocomposites: A comparison of TGA and laser pulse heating, Polym. Degrad. Stab. 141 (2017) 41–44, https://doi.org/10.1016/j.polymdegradstab.2017.05.006.

[31] S.F. Bartolucci, M. Miller, J. Warrender, Infrared laser ablation of polymeric nanocomposites: A study of surface structure and plume formation, J Appl Phys 120 (2) (2016), https://doi.org/10.1063/1.4971260.

[32] S.W. Allison, G.T. Gillies, Remote thermometry with thermographic phosphors: Instrumentation and applications, Rev. Sci. Instrum. 68 (7) (1997) 2615–2650, https://doi.org/10.1063/1.1148174.

[33] J.M. Chalmers, W.F. Gaskin, M.W. Mackenzie, Crystallinity in poly(aryl-ether-ketone) plaques studied by multiple internal reflection spectroscopy, Polym. Bull. 11 (1984) 433–435, https://doi.org/10.1007/BF00265483.

[34] A.F.H. Kaplan, Analysis and modeling of a high-power YB:fiber laser beam profile, Opt. Eng. 50 (5) (2011) 054201, https://doi.org/10.1117/1.3580660.

[35] R. Tian, G. Zhu, Y. Lv, T. Wu, T. Ren, Z. Ma, S. Zhang, Experimental study and numerical simulation for the interaction between laser and PEEK with different crystallinity, High Perform. Polym. 33 (8) (2021) 851–861, https://doi.org/10.1177/0954008321996771.

[36] T. Bayerl, M. Duhovic, P. Mitschang, D. Bhattacharyya, The heating of polymer composites by electromagnetic induction - A review, Composites Part A: Applied Science and Manufacturing 57 (2014) 27–40, https://doi.org/10.1016/j.compositesa.2013.10.024.

[37] J. M. Chalmers, N. J. Everall, K. Hewitson, M. A. Chesters, M. Pearson, A. Grady, B. Ruzicka, Fourier transform infrared microscopy: Some advances in techniques for characterisation and structureproperty elucidations of industrial material, Analyst 123 (1998) 579–586, https://doi.org/10.1039/A707070E.

[38] J. Chalmers, N. Everall, S. Ellison, Specular reflectance: A conventional tool for polymer characterization by FTIR-microscopy? Micron 27 (5) (1996) 315–328, https://doi.org/10.1016/S0968-4328(96)00021-2.

[39] M. Regis, A. Bellare, T. Pascolini, P. Bracco, Characterization of thermally annealed PEEK and CFR-PEEK composites: Structure-properties relationships, Polym. Degrad. Stab. 136 (2017) 121–130, https://doi.org/10.1016/j.polymdegradstab.2016.12.005.

[40] S. Hammouti, B. Beaugiraud, M. Salvia, C. Mauclair, A. Pascale-Hamri, S. Benayoun, S. Valette, Elaboration of submicron structures on PEEK polymer by femtosecond laser, Appl Surf Sci 327 (2015) 277–287, https://doi.org/10.1016/j.apsusc.2014.11.163.

[41] American Society for Testing and Materials (ASTM), Standard test method for measurement of percent crystallinity of polyetheretherketone (PEEK) polymers by means of specular reflectance Fourier transform infrared spectroscopy (R-FTIR), Annual Book of ASTM Standards. (2020), https://doi.org/10.1520/F2778-09R20.

[42] M. Doumeng, L. Makhlouf, F. Berthet, O. Marsan, K. Delb, J. Denape, F. Chabert, A comparative study of the crystallinity of polyetheretherketone by using density, DSC, XRD, and Raman spectroscopy techniques, Polym Test 93 (2021) 106878, https://doi.org/10.1016/j.polymertesting.2020.106878.

[43] J. Agbenyega, G. Ellis, P. Hendra, W. Maddams, C. Passingham, H. Willis, J. Chalmers, Applications of Fourier transform Raman spectroscopy in the synthetic polymer field, Spectrochimica Acta Part A: Molecular Spectroscopy 46 (2) (1990) 197–216, https://doi.org/10.1016/0584-8539(90)80090-L.

[44] B. Stuart, The application of Fourier transform Raman spectroscopy to polymer tribology, Spectrochim. Acta, Part A 53 (1) (1997) 111–118, https://doi.org/10.1016/S1386-1425(97)83015-6.

[45] M. Doumeng, F. Ferry, K. Delb, T. Mrian, F. Chabert, F. Berthet, O. Marsan, V. Nassiet, J. Denape, Evolution of crystallinity of PEEK and glass-fibre reinforced PEEK under tribological conditions using Raman spectroscopy, Wear 426–427 (2019) 1040–1046, https://doi.org/10.1016/j.wear.2018.12.078.

[46] N. Everall, J. Chalmers, R. Ferwerda, J. van der Maas, P. Hendra, Measurement of poly(aryl ether ether ketone) crystallinity in isotropic and uniaxial samples using Fourier transform Raman spectrocopy: A comparison of univariate and partial leastsquares calibrations, J. Raman Spectrosc. 25 (1) (1994) 43–51, https://doi.org/10.1002/jrs.1250250107.

[47] B. Briscoe, B. Stuart, P. Thomas, D. Williams, A comparison of thermal- and solvent-induced relaxation of poly(ether ether ketone) using Fourier transform

[48] G. Ellis, M. Naffakh, C. Marco, P. Hendra, Fourier transform Raman spectroscopy in the study of technological polymers part 1: Poly(aryl ether ketones), their composites and blends, Spectrochim. Acta, Part A 53 (13) (1997) 2279–2294, https://doi.org/10.1016/S1386-1425(97)00168-6.

[49] J. Louden, Crystallinity in poly(aryl ether ketone) films studied by Raman spectroscopy, Polymer communications Guildford 27 (3) (1986) 82–84.

[50] M. Hardiman, T. Vaughan, C. McCarthy, A review of key developments and pertinent issues in nanoindentation testing of fibre reinforced plastic microstructures, Compos Struct 180 (2017) 782–798, https://doi.org/10.1016/j.compstruct.2017.08.004.

[51] R.F. Gibson, A review of recent research on nanoindentation of polymer composites and their constituents, Compos Sci Technol 105 (2014) 51–65, https://doi.org/10.1016/j.compscitech.2014.09.016.

[52] M. Hardiman, T. Vaughan, C. McCarthy, Fibrous composite matrix characterisation using nanoindentation: The effect of fibre constraint and the evolution from bulk to in-situ matrix properties, Composites Part A: Applied Science and Manufacturing 68 (2015) 296–303, https://doi.org/10.1016/j.compositesa.2014.09.022.

[53] M. Rodrguez, J. Molina-Aldareguia, C. Gonzlez, J. LLorca, Determination of the mechanical properties of amorphous materials through instrumented nanoindentation, Acta Mater 60 (9) (2012) 3953–3964, https://doi.org/10.1016/j.actamat.2012.03.027.

[54] D. Tranchida, S. Piccarolo, J. Loos, A. Alexeev, Mechanical characterization of polymers on a nanometer scale through nanoindentation. A study on pile-up and viscoelasticity, Macromolecules 40 (4) (2007) 1259–1267, https://doi.org/10.1021/ma062140k.

[55] F. Naya, C. Gonzlez, C. Lopes, S.V. der Veen, F. Pons, Computational micromechanics of the transverse and shear behavior of unidirectional fiber reinforced polymers including environmental effects, Composites Part A: Applied Science and Manufacturing 92 (2017) 146–157, https://doi.org/10.1016/j.compositesa.2016.06.018.

[56] J.R. Gregory, S. Spearing, Nanoindentation of neat and in situ polymers in polymermatrix composites, Compos Sci Technol 65 (3) (2005) 595–607, https://doi.org/10.1016/j.compscitech.2004.09.001.

[57] M. Hardiman, T. Vaughan, C. McCarthy, The effects of pile-up, viscoelasticity and hydrostatic stress on polymer matrix nanoindentation, Polym Test 52 (2016) 157–166, https://doi.org/10.1016/j.polymertesting.2016.04.003.

[58] G.Z. Voyiadjis, A. Samadi-Dooki, L. Malekmotiei, Nanoindentation of high performance semicrystalline polymers: A case study on PEEK, Polym Test 61 (2017) 57–64, https://doi.org/10.1016/j.polymertesting.2017.05.005.

[59] J.C. Hay, A. Bolshakov, G.M. Pharr, Critical examination of the fundamental relations used in the analysis of nanoindentation data, J Mater Res 14 (6) (1999) 2296–2305, https://doi.org/10.1557/JMR.1999.0306.

[60] W.C. Oliver, G.C. Pharr, An improved technique for determining hardness and elastic modulus using load and displacement sensing indentation experiments, J Mater Res 7 (6) (1992) 1564–1583, https://doi.org/10.1557/JMR.1992.1564.

[61] X. Li, B. Bhushan, A review of nanoindentation continuous stiffness measurement technique and its applications, Mater Charact 48 (1) (2002) 11–36, https://doi.org/10.1016/S1044-5803(02)00192-4.

[62] A. Jonas, R. Legras, J.-P. Issi, Differential scanning calorimetry and infra-red crystallinity determinations of poly(aryl ether ether ketone), Polymer 32 (18) (1991) 3364–3370, https://doi.org/10.1016/0032-3861(91)90540-Y.

[63] A.G. Al Lafi, FTIR Spectroscopic analysis of ion irradiated poly (ether ether ketone), Polym. Degrad. Stab. 105 (2014) 122–133, https://doi.org/10.1016/j.polymdegradstab.2014.04.005.

[64] B. Stuart, B. Briscoe, A Fourier transform Raman spectroscopy study of poly (ether ether ketone)/polytetrafluoroethylene (PEEK/PTFE) blends, Spectrochimica Acta Part A: Molecular Spectroscopy 50 (11) (1994) 2005–2009, https://doi.org/10.1016/0584-8539(94)80212-2.

[65] A. Ramgobin, G. Fontaine, S. Bourbigot, A case study of polyether ether ketone (I): Investigating the thermal and fire behavior of a high-Performance material, Polymers (Basel) 12 (8) (2020), https://doi.org/10.3390/polym12081789.

[66] D. Wu, Q. Miao, Z. Dai, F. Niu, G. Ma, Effect of voids and crystallinity on the interlaminar shear strength of in-situ manufactured CF/PEEK laminates using repass treatment, Compos Sci Technol 224 (2022) 109448, https://doi.org/10.1016/j.compscitech.2022.109448.

[67] F. Shadmehri, S.V. Hoa, J. Fortin-Simpson, H. Ghayoor, Effect of in situ treatment on the quality of flat thermoplastic composite plates made by automated fiber placement (AFP), Advanced Manufacturing: Polymer & Composites Science 4 (2) (2018) 41–47, https://doi.org/10.1080/20550340.2018.1444535.